

Materials and noncoplanar mesh designs for integrated circuits with linear elastic responses to extreme mechanical deformations

Dae-Hyeong Kim^a, Jizhou Song^b, Won Mook Choi^c, Hoon-Sik Kim^a, Rak-Hwan Kim^a, Zhuangjian Liu^d, Yonggang Y. Huang^{e,1}, Keh-Chih Hwang^f, Yong-wei Zhang^{d,g}, and John A. Rogers^{a,h,1}

^aDepartments of Materials Science and Engineering, Beckman Institute, and Frederick Seitz Materials Research Laboratory, and ^bDepartments of Chemistry and Electrical and Computer Engineering, University of Illinois at Urbana-Champaign, 1304 West Green Street, Urbana, IL 61801; ^cDepartment of Mechanical and Aerospace Engineering, University of Miami, Coral Gables, FL 33146; ^dSamsung Advanced Institute of Technology, Mt. 14-1 Nongseong-Dong, Giheung-Gu, Yongin-Si, Gyeonggi-Do 449-712, Republic of Korea; ^eInstitute of High Performance Computing, 1 Fusionopolis Way, #16-16 Connexis, Singapore 138632; ^fDepartments of Civil and Environmental Engineering and Mechanical Engineering, Northwestern University, Evanston, IL 60208; ^gDepartment of Engineering Mechanics, Tsinghua University, Beijing 100084, China; and ^hDepartment of Materials Science and Engineering, National University of Singapore, Singapore 119260

Edited by George M. Whitesides, Harvard University, Cambridge, MA, and approved September 30, 2008 (received for review August 1, 2008)

Electronic systems that offer elastic mechanical responses to high-strain deformations are of growing interest because of their ability to enable new biomedical devices and other applications whose requirements are impossible to satisfy with conventional wafer-based technologies or even with those that offer simple bendability. This article introduces materials and mechanical design strategies for classes of electronic circuits that offer extremely high stretchability, enabling them to accommodate even demanding configurations such as corkscrew twists with tight pitch (e.g., 90° in ≈1 cm) and linear stretching to “rubber-band” levels of strain (e.g., up to ≈140%). The use of single crystalline silicon nanomaterials for the semiconductor provides performance in stretchable complementary metal-oxide-semiconductor (CMOS) integrated circuits approaching that of conventional devices with comparable feature sizes formed on silicon wafers. Comprehensive theoretical studies of the mechanics reveal the way in which the structural designs enable these extreme mechanical properties without fracturing the intrinsically brittle active materials or even inducing significant changes in their electrical properties. The results, as demonstrated through electrical measurements of arrays of transistors, CMOS inverters, ring oscillators, and differential amplifiers, suggest a valuable route to high-performance stretchable electronics.

flexible electronics | stretchable electronics | semiconductor nanomaterials | plastic electronics | buckling mechanics

Increasingly important classes of application exist for electronic systems that cannot be formed in the usual way, on semiconductor wafers. The most prominent example is in large-area electronics (e.g., back planes for liquid crystal displays), where overall system size rather than operating speed or integration density, is the most important metric. Similar systems that use flexible substrates are presently the subject of widespread research and commercialization efforts because of advantages that they offer in durability, weight, and ease of transport/use (1, 2). Stretchable electronics represents a fundamentally different and even more challenging technology, of interest for its unique ability to flex and conform to complex curvilinear surfaces such as those of the human body. Several promising approaches exist, ranging from the use of stretchable interconnects between rigid amorphous silicon devices (3) to “wavy” layouts in single-crystalline silicon CMOS circuits (4), both on elastomeric substrates, to net-shaped structures in organic electronics on plastic sheets (5). None offers, however, the combination of electrical performance (high electron and hole mobility), scalability (with relatively modest modifications to conventional microelectronic technologies), integrated circuit applicability in complementary designs and mechanical properties required of some of the most demanding, and most interesting, systems. Here, we introduce

design concepts for stretchable electronics that exploit semiconductor nanomaterials (i.e., silicon ribbons) in ultrathin, mechanically neutral circuit layouts integrated on elastomeric substrates in noncoplanar mesh designs, with certain features inspired by methods recently reported for transforming planar optoelectronics into hemispherical shapes for electronic-eye cameras (6). The noncoplanar structure, combined with deformable serpentine bridge designs, can accomplish much higher stretchability (i.e., up to ≈140%) compared with previous reports of related systems (3–6). This increased stretchability enables much wider application possibilities, including electronic circuits on complex surfaces with high curvature. As demonstrated in diverse circuit examples, these ideas accomplish a form of stretchable electronics that uniquely offers both high performance and an ability to accommodate nearly any type of mechanical deformation to high levels of strain. Experimental and theoretical studies of the electrical and mechanical responses illuminate the key materials and physics aspects associated with this type of technology.

Results and Discussion

Fig. 1A schematically illustrates steps for fabricating a representative system that consists of a square array of CMOS inverters. The overall process can be divided into 2 parts. The first defines CMOS circuits on ultrathin plastic substrates by using printing methods and single-crystalline silicon ribbons, according to procedures described previously (7). For all of the results reported here, the ribbons had thicknesses of 260 nm and 290 nm for p-channel and n-channel metal oxide semiconductor field effect transistors (MOSFETs), respectively. The gate dielectric consisted of a 50-nm-thick layer of SiO₂ deposited by plasma-enhanced chemical-vapor deposition. The same type of film formed an interlayer dielectric for metal (Ti:5 nm/Au:150 nm) interconnect lines and electrodes. The plastic substrate consisted of a thin layer (1.2 μm) of polyimide (PI) supported by a carrier wafer (test grade silicon) coated with a film (100 nm) of poly(methylmethacrylate) (PMMA) (8). A thin top coating of

Author contributions: D.-H.K., J.S., W.M.C., Y.Y.H., and J.A.R. designed research; D.-H.K., J.S., H.-S.K., R.-H.K., Z.L., Y.Y.H., and J.A.R. performed research; D.-H.K., J.S., Z.L., Y.Y.H., K.-C.H., Y.-w.Z., and J.A.R. analyzed data; and D.-H.K., J.S., Z.L., Y.Y.H., and J.A.R. wrote the paper.

The authors declare no conflict of interest.

This article is a PNAS Direct Submission.

Freely available online through the PNAS open access option.

¹To whom correspondence may be addressed. E-mail: jrogers@uiuc.edu or y-huang@northwestern.edu.

This article contains supporting information online at www.pnas.org/cgi/content/full/0807476105/DCSupplemental.

© 2008 by The National Academy of Sciences of the USA

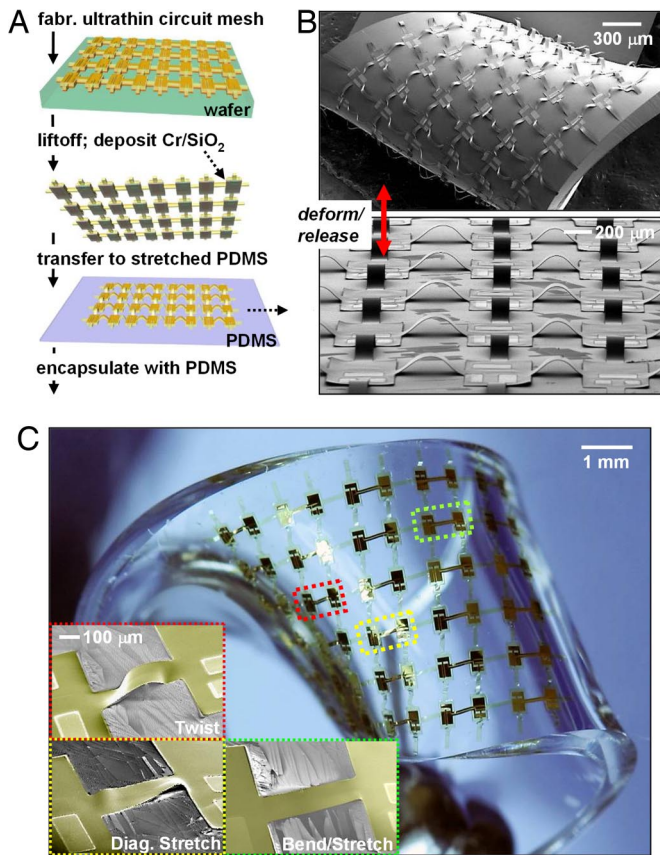


Fig. 1. Fabrication of noncoplanar stretchable electronics and responses to deformation. (A) Schematic overview of the fabrication process for representative circuits that accomplish high levels of stretchability through the use of noncoplanar mesh designs integrated with elastomeric substrates [for the case shown here, PDMS]. (B) SEM images of an array of CMOS inverters that result from this process, in an undeformed state (*Lower*; $\approx 20\%$ prestrain) and in a corresponding configuration that results from a complex twisting motion (*Upper*). (C) Optical image of a freely deformed stretchable array of CMOS inverters, highlighting 3 different classes of deformation: diagonal stretching, twisting, and bending. The *Insets* provide SEM images for each case (colorized for ease of viewing).

PI (1.2 μm), with etched (reactive ion etching; RIE) holes for electrical access, protected the circuits and placed the most fragile components near the neutral mechanical plane (4). Individual devices fabricated in this manner exhibited device mobilities of ≈ 130 and ≈ 370 cm^2/Vs for p-channel and n-channel MOSFETs, respectively, with on/off ratios $>10^6$ and operating voltages in the range of <5 V. These fabrication procedures are useful but have some disadvantages. For example, conventional self-aligned processes for defining the channel and gate cannot be implemented easily. The polymer materials restrict the processing temperatures and prevent, as an example, the use of dry oxide for the gate dielectric. A modified procedure, in which most or all of the device or circuit block processing occurs on the mother silicon wafer, before transfer to the polymer substrate, can avoid these limitations. Exploring this possibility represents a focus of current work.

The second part of the fabrication process involves structuring the circuits into noncoplanar layouts intimately integrated with elastomeric substrates to yield systems with reversible, elastic responses to extreme mechanical deformations. In the first step toward achieving this outcome, certain regions of the PI/PMMA between the electronic components of the system were removed by RIE through a patterned layer of photoresist. The result was

a segmented mesh with active device islands connected electrically and/or mechanically by thin polymer bridges with or without metal-interconnect lines, respectively. Immersion in acetone washed away the PMMA layer to release the system from the carrier. Lifting off the patterned circuit sheet onto a slab of poly(dimethylsiloxane) (PDMS) exposed its underside for deposition of a thin layer of Cr/SiO₂ (3 nm/30 nm) at the locations of the islands by electron beam evaporation through an aligned shadow mask. Delivering the circuit to a biaxially prestrained substrate of PDMS with its surface activated by exposure to ozone led to the formation of strong mechanical bonds at the positions of the islands. The interface chemistry responsible for this bonding involves condensation reactions between hydroxyl groups on the SiO₂ and PDMS (4) to form —O—Si—O— linkages, similar to that described recently for controlled buckling in collections of semiconductor ribbons (8). Releasing the prestrain resulted in compressive forces that caused the connecting bridges to lift vertically off the PDMS, thereby forming arc-shaped structures. We refer to this layout as a noncoplanar mesh design. The localization of this out-of-plane mechanical response to the bridges results partly from their poor adhesion to the PDMS and partly from their narrow geometries and low bending stiffnesses compared with the device islands. (This latter aspect allows similar structures to be formed even without the patterned SiO₂ adhesion layer.) The bottom frames of Fig. 1A and B show schematic illustrations and scanning electron microscope (SEM) images. In this format, the system can be stretched or compressed to high levels of strain (up to 100%, and in some cases higher, as described subsequently), in any direction or combination of directions both in and out of the plane of the circuit, as might be required to allow complex twisting, shearing, and other classes of deformation. Fig. 1B *Upper* and Fig. 1C *Upper* show images that illustrate some of these capabilities in circuits that use a PDMS substrate with thickness ≈ 1 mm and a prestrain of $\approx 17\%$, as defined by the change in separation between inner edges of adjacent device islands. For practical applications, such systems are coated with a protective layer of PDMS in a way that does not alter significantly the mechanical properties, as argued subsequently. For ease of imaging and electrical probing, the circuits described in the following are all unencapsulated.

The physics of deformation associated with applying tensile or compressive forces oriented along the directions of the bridges is similar to that involved in relaxing the prestrain in the circuit-fabrication process of Fig. 1. The bridges move up or down (corresponding to decreases or increases in end-to-end lengths, respectively) as the system is compressed or stretched, respectively. Another, less obvious, feature is that the thin, narrow construction of these bridges also enables them to twist and shear in ways that can accommodate more complex distributions of strain. Fig. 1C shows some representative cases, described in more detail subsequently, for different regions of a system under a complex, twisting deformation. The basic mechanics is similar to that of systems that are encapsulated by PDMS. For example, calculation indicates that the maximum strain that can be applied to the system, as shown in Fig. 1B *Lower*, reduces by only $\approx 2.5\%$ because of the addition of a ≈ 1 -mm-thick overcoat of PDMS [supporting information (SI) Fig. S1].

These designs lead to electronic properties that are largely independent of strain, even in extreme configurations such as those illustrated in Fig. 1B and C. This feature can be demonstrated explicitly through device and circuit measurements on systems for various, well-defined mechanical deformations induced with custom assemblies of mechanical stages. The simplest case corresponds to in-plane stretching in directions parallel to the bridges. Testing of this deformation mode was performed by using 3-stage ring oscillators, in which each island supports an n

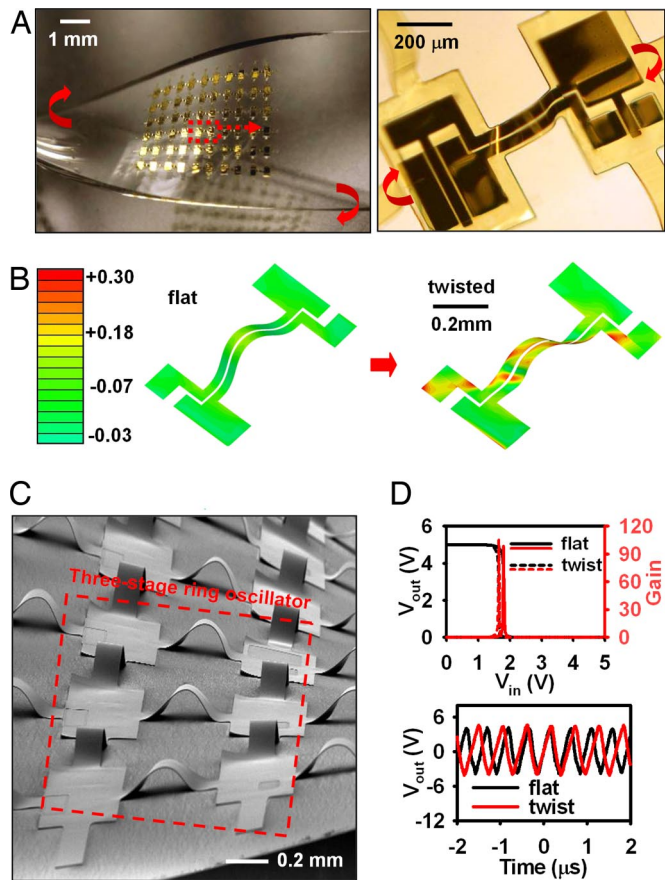


Fig. 3. Mechanical and electrical responses of noncoplanar stretchable electronics to twisting deformations. (A) Optical images of an array of stretchable CMOS inverters in a twisted configuration (Left) and magnified view of a single inverter, illustrating the nature of the deformation (Right). (B) FEM simulation of the mechanics of twisting on the bridge structures. (C) SEM image of an array of stretchable, 3-stage CMOS ring oscillators in a twisted configuration. (D) Electrical characteristics of the inverters (Upper; gain and output voltage, V_{out} , as a function of input voltage, V_{in}) and oscillators (Lower; output voltage, V_{out} , as a function of time) in planar and twisted states.

An extreme type of deformation, which is partly involved in the configuration shown in Fig. 1, involves twisting into corkscrew shapes with tight pitch. Under such applied strain, the bridges deform due mainly to in-plane shear with a magnitude on the order of the ratio of (bridge or island) thickness to length times the rotation angle (see *SI Text* for details). Such twisting deformation is different from off-axis stretching because it does not involve buckling and is therefore amenable to linear analysis. For a 90° rotation over a distance corresponding to a pair of bridges and an island, the maximum shear strains in the metal and Si layers are 0.08% and 0.02%, respectively, for the 445- μm -long bridge and 260- μm -long island. Fig. 3A Left shows an image of a circuit on thin PDMS, in a twisted geometry; Fig. 3A Right shows a magnified view of a CMOS inverter in this system. As for the previously described cases, FEM simulation (Fig. 3B) supports the experimental observations and reveals the level of principal strain to be 0.3% in the metal layer of the bridge and the island. A SEM image of an interconnected array of inverters for a ring oscillator (Fig. 3C) shows the shape of the twisted bridges. Electrical measurements indicate stable electrical performance before and after twisting, both for inverters (Fig. 3D Upper) and ring oscillators (Fig. 3D Lower). The electrical properties, in all cases, are comparable with those described previously. In other words, the systems are, to within experi-

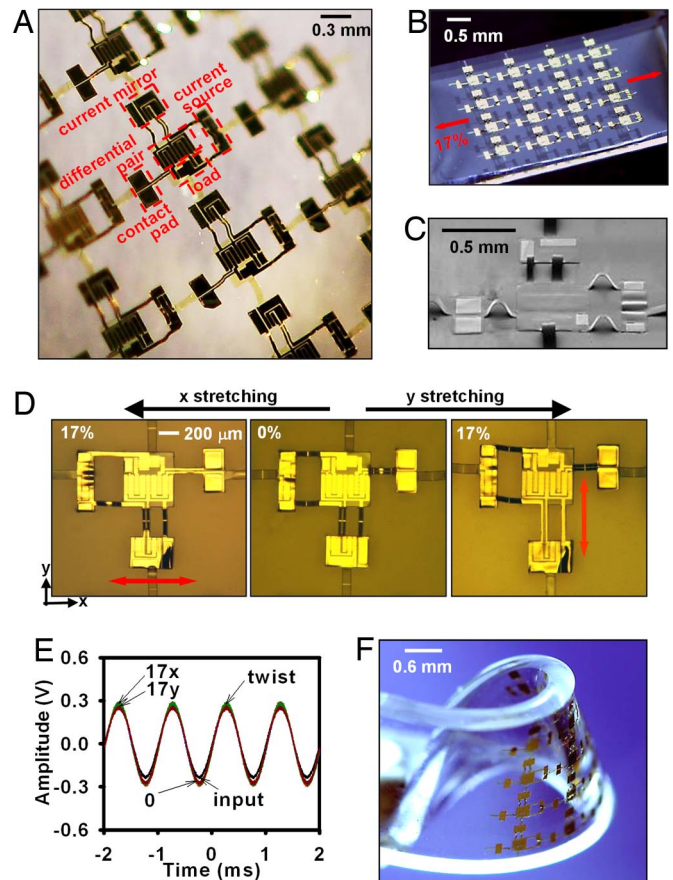


Fig. 4. Noncoplanar stretchable electronics with asymmetric layouts. (A and B) Optical images of an array of stretchable differential amplifiers in twisted (A) and planar stretched (B) layouts. (C) Tilted view SEM of a representative amplifier, showing the noncoplanar layout. (D and E) Optical images under stretching along the x and y directions (D) and corresponding electrical output as a function of time for a sinusoidal input (E). (F) Optical image of a device in a complex deformation mode. Here, 17x and 17y refer to 17% tensile strains along the x and y directions indicated in D, respectively.

mental uncertainty, agnostic to deformation mode for all configurations studied here.

Figs. 1–3 illustrate examples for circuits, such as inverters and ring oscillators, that are straightforward to implement in repetitive, arrayed layouts. More complex, irregular designs might be required in many cases of practical importance; these can also be implemented in noncoplanar mesh designs. We demonstrated this concept for a differential amplifier (10), in which we divided the circuit into 4 sections, each of which forms an island connected by metal lines on pop-up bridges. The red dotted boxes in Fig. 4A Left highlight these 4 regions; an angled view SEM image in the *Inset* shows the structure. The bridges provide a mechanics that is conceptually similar to those in the regular array layouts, even though the details are somewhat different. As a result, this irregular circuit can be stretched or twisted reversibly, as shown in Fig. 4B and C, respectively. Fig. 4D shows magnified images of stretching in the x and y directions. Electrical measurements verify that the amplifiers work well under these deformations. The gains for 0%, 17% x stretching, 17% y stretching, and twisting to a full 180° rotation of a PDMS substrate with a length of ≈ 2 cm were 1.15, 1.12, 1.15, and 1.09 (design value ≈ 1.2), respectively. Such systems can also be freely deformed, as shown in Fig. 4F.

Although the materials and mechanical designs described previously can accommodate larger strains and in more diverse

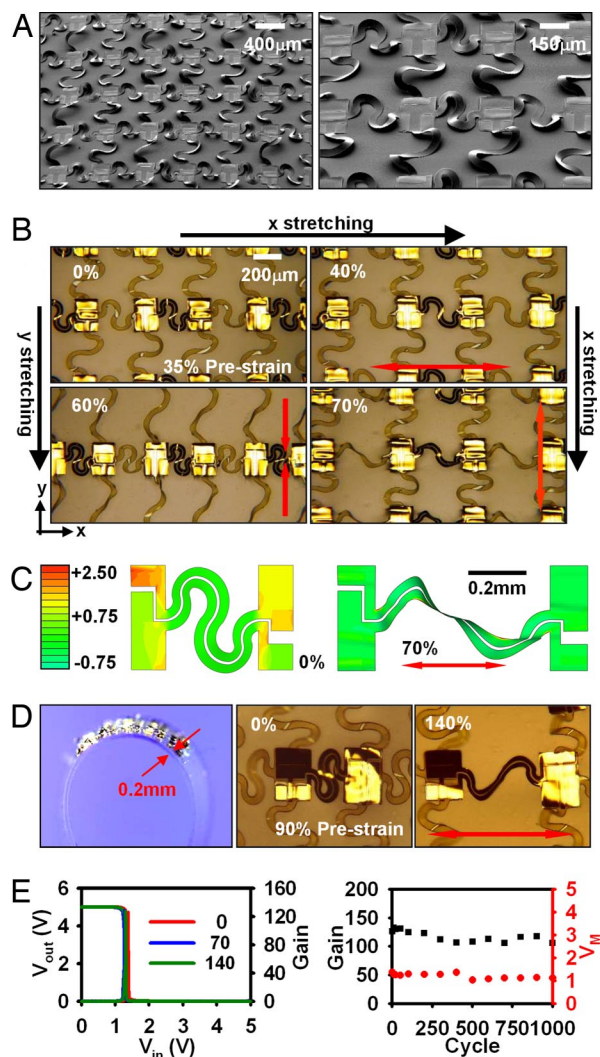


Fig. 5. Extreme stretchability in noncoplanar electronics with serpentine bridge designs. (A) SEM image of an array of stretchable CMOS inverters with noncoplanar bridges that have serpentine layouts (Left) and magnified view (Right). (B) Optical images of stretching tests in the x and y directions. (C) FEM simulation before (35% prestrain) and after (70% applied strain) stretching. (D) Arrays of inverters on a thin PDMS substrate (0.2 mm) (Left) and images in unstretched (middle; 90% prestrain) and stretched (Right; 140% tensile strain) states. (E) Transfer characteristics and gain for a representative inverter under stretching (Left) and plot of gain and voltage at maximum gain (V_M) for a similar device as a function of stretching cycles (Right).

configurations compared with previous demonstrations, they might not satisfy requirements for certain advanced device concepts, such as electronics for “smart” surgical gloves or hemispherical focal plane arrays with large, double curvature, where truly “rubber band-like” stretchability (e.g., to $>50\%$ strain) is needed. A simple method to increase the stretchability, without changing the materials or layouts in the stacks that make up the circuits, involves increasing the separations between the device islands and decreasing the thicknesses of the bridges. The quantitative effects of these parameters on the peak material strain can be represented by a simple analytical relation, presented in the SI, for the approximate case that the islands are strictly rigid and remain planar (Fig. S5). To expand the deformability even further, without increasing the sparseness of the distribution of islands, serpentine bridges can be used. Fig. 5A shows SEM images of such a design after executing the fabrication procedures of Fig. 1. When external strain is applied along

the x or y directions, these noncoplanar serpentine bridges effectively compensate the applied strain not only through changes in height but also by changes in geometry of the serpentine shape. Fig. 5B shows images of the response of a representative device to on-axis stretching strains up to 70%, for a system built with 35% prestrain, in which deformations of the serpentine bridges exhibit changes in configurations that might be expected intuitively. Remarkably, finite-element modeling reveals that, even to stretching strains of 70%, the peak strains in the metal layer in the bridges and islands are 0.2% and 0.5%, respectively, and the strain in silicon is 0.15% as indicated in Fig. 5C. (The strains reach $\approx 3\%$ in certain locations of the PI.) To explore the limits, we used thin PDMS substrates (0.2 mm) to facilitate stretching to even larger strains. Fig. 5D shows a case corresponding to $\approx 90\%$ prestrain, which allows stretching to $\approx 140\%$ strain and corresponds to $\approx 100\%$ system strain. The large prestrain improves the stretchability, and it also increases the active-area density in the circuit by decreasing the lengths of the interconnecting bridges. For example, in the designs illustrated here, the active-area density for a prestrain of $\approx 35\%$ (Fig. 5B, $\approx 70\%$ stretchability) and $\approx 90\%$ (Fig. 5D, $\approx 140\%$ stretchability) is $\approx 19\%$ and $\approx 34\%$, respectively. The essential strategy of bridge-type interconnects, however, requires a tradeoff between degree of stretchability and area consumed by the interconnects. Consistent with the small strains in the active materials revealed by FEM, the electrical properties approach those of the corresponding unstrained, planar systems; the operation is also stable over many cycles (up to 1,000, evaluated here) of stretching, as indicated in Fig. 5E.

Finally, the practical application of pop-up circuits requires an additional encapsulation layer on top of devices to protect active regions from unwanted damage. To this end, we coated the circuits with a liquid prepolymer PDMS and cured it after all bridges and islands were embedded. A dual neutral mechanical plane design can be implemented by controlling the top and bottom PDMS thickness to provide additional mechanical strength for deformation (4). This encapsulation has relatively minor effects on the essential mechanics, primarily through slight increases in the strain in the bridges due to restricted deformation inside the PDMS. Pop-up inverters with straight (Movie S1 and Movie S2) and S-shaped (Movie S3 and Movie S4) bridges show these behaviors (see also SI Text).

Conclusions

Collectively, the results presented here provide design rules for circuits that offer both excellent electrical performance and capacities to be elastically deformed in diverse configurations to high levels of strain. The same ideas can, in many cases, be used to advantage in other conventionally rigid, planar technologies such as photovoltaics, microfluidics, sensor networks, photonics, and others. These and related types of systems might enable many important new applications that cannot be addressed with other approaches. Exploring these possibilities represents a fruitful area for future work.

Materials and Methods

Preparation of Doped Silicon Ribbons. Preparation of doped silicon ribbons starts with the doping of the top silicon on silicon-on-insulator (SOI) wafers: nMOS source/drain doping with p-type SOI wafers (SOITEC) and pMOS source/drain doping with n-type SOI wafers (SOITEC). This process uses plasma-enhanced chemical-vapor deposition (PECVD) of silicon dioxide (SiO_2) for a diffusion mask, photolithography, and RIE with CF_4/O_2 gas for patterning, spin coating, and high-temperature diffusion of boron spin-on dopant (B153; Filmtronics) at $1,000^\circ\text{C}$ to $\approx 1,050^\circ\text{C}$ for p-type and phosphorous spin-on dopant (P509; Filmtronics) at 950°C to $\approx 1,000^\circ\text{C}$ for n-type. The typical surface doping concentrations using phosphorous and boron spin-on dopants are $\approx 2 \times 10^{20} \text{ cm}^{-3}$ and $\approx 10^{20} \text{ cm}^{-3}$, respectively (13, 14). After doping, ribbons are defined by photolithography and RIE; they are released from the mother wafer by removing the buried oxide layer of the SOI wafers. These

Supporting Information

Kim *et al.* 10.1073/pnas.0807476105

SI Text

Encapsulation Case. The noncoplanar bridges can be protected by encapsulation with a top, spin-cast layer of PDMS. The post-buckling analysis of bridges and islands is coupled. The out-of-displacement in each region has its own wavelength and amplitude, and across the regions, the displacement, rotation, moment, and shear force are continuous. The minimization of total energy, which consists of the bending and membrane energy of the bridges and the islands, and the strain energy in the substrate gives the wavelength and amplitudes in all regions. For example, for a system level applied strain of -20% when the prestrain is 10.7% , the amplitude of bridges is $196\ \mu\text{m}$, whereas that of islands is only $1\ \mu\text{m}$.

Fig. S1 shows the maximum strains in different device layers versus the system-level applied strain. The encapsulated system fails before the applied strain reaches the prestrain, which is different from that without capsulation (i.e., the prestrain plus 1% or 2% of fracture strain of materials).

Effective Tensile and Bending Stiffness of Multilayer Stacks. Fig. S2 shows multilayer stacks with the first layer on top and n th layer at the bottom. Their (plane-strain) moduli and thicknesses are denoted by $\bar{E}_1, \dots, \bar{E}_n$ and h_1, \dots, h_n , respectively. The length and width are denoted by L_s and W_s . The multilayer stacks are modeled as a composite beam with the effective tensile stiffness (1)

$$\bar{EA} = w_s \sum_{i=1}^n \bar{E}_i h_i, \quad [1]$$

and effective bending stiffness (1)

$$\begin{aligned} \bar{EI} = w_s \left[\sum_{i=1}^n \bar{E}_i h_i \left(b - \sum_{j=1}^i h_j \right)^2 + \sum_{i=1}^n \bar{E}_i h_i^3 \left(b - \sum_{j=1}^i h_j \right) \right. \\ \left. + \frac{1}{3} \sum_{i=1}^n \bar{E}_i h_i^3 \right], \quad [2] \end{aligned}$$

where b is the distance between the neutral mechanical plane to the top surface, and is given by (1)

$$b = \frac{\sum_{i=1}^n \bar{E}_i h_i \left[\left(\sum_{j=1}^i h_j \right) - \frac{h_i}{2} \right]}{\sum_{i=1}^n \bar{E}_i h_i}. \quad [3]$$

Noncoplanar Bridges Between Islands. The nature of compressibility obtained from the noncoplanar bridges connecting the adjacent islands, shown by the SEM image in Fig. 1B, can be understood through theoretical analysis (see Fig. S3A). The bridges ($n = 4$, PI/metal/SiO₂/PI: $\approx 1.2\ \mu\text{m}/0.15\ \mu\text{m}/0.05\ \mu\text{m}/1.2\ \mu\text{m}$) are modeled as a composite beam with the effective tensile \bar{EA}_{bridge} and bending stiffness \bar{EI}_{bridge} obtained from Eqs. 1 and 2 for $n = 4$. The elastic moduli and Poisson's ratios are $E_{\text{SiO}_2} = 70\ \text{GPa}$, $\nu_{\text{SiO}_2} = 0.17$, $E_{\text{metal}} = 78\ \text{GPa}$, $\nu_{\text{metal}} = 0.44$, $E_{\text{PI}} = 2.5\ \text{GPa}$, and $\nu_{\text{PI}} = 0.34$.

The out-of-plane displacement, u , of the non-coplanar bridges

$$\text{takes the form } u = \frac{A}{2} \left(1 + \cos \frac{2\pi}{L_{\text{bridge}}} z \right),$$

which satisfies vanishing displacement and slope at the 2 ends ($z = \pm L_{\text{bridge}}/2$), where A is the amplitude, x is the position along the bridge and L_{bridge} is the lateral separation distance between adjacent islands. The initial distance $L_{\text{bridge}}^0 = 445\ \mu\text{m}$ is measured in the as-fabricated configuration. The in-plane displacement can then be obtained from the force equilibrium. These give the bending energy

$$U_b = \bar{EI}_{\text{bridge}} \frac{\pi^4 A^2}{(L_{\text{bridge}}^0)^3}$$

and membrane energy

$$U_m = \frac{1}{2} \bar{EA}_{\text{bridge}} \left[\frac{\pi^2 A^2}{4(L_{\text{bridge}}^0)^2} - \frac{L_{\text{bridge}}^0 - L_{\text{bridge}}}{L_{\text{bridge}}^0} \right]^2 L_{\text{bridge}}^0.$$

Energy minimization

$$\frac{\partial(U_b + U_m)}{\partial A} = 0$$

yields an analytical expression for the amplitude

$$A = \frac{2L_{\text{bridge}}^0}{\pi} \sqrt{\frac{L_{\text{bridge}}^0 - L_{\text{bridge}}}{L_{\text{bridge}}^0} - \varepsilon_c},$$

$$\text{where } \varepsilon_c = \frac{\bar{EI}_{\text{bridge}} 4\pi^2}{\bar{EA}_{\text{bridge}} L_{\text{bridge}}^0}$$

is the critical buckling strain, and is 0.0034% for the system shown above. For $L_{\text{bridge}} = 370\ \mu\text{m}$, the analytical expression above give the amplitude $A = 116.3\ \mu\text{m}$, which agrees well with the experiment's $A = 115\ \mu\text{m}$. The corresponding maximum strain in the metal layer of the bridge is $\approx 0.11\%$, substantially below the fracture strain for the metal.

Strain Distributions in Islands. The islands ($n = 5$, PI/metal/SiO₂/Si/PI: $\approx 1.2\ \mu\text{m}/0.15\ \mu\text{m}/0.05\ \mu\text{m}/0.25\ \mu\text{m}/1.2\ \mu\text{m}$) are modeled as a composite plate with the effective tensile stiffness $\bar{EA}_{\text{islands}}$ and effective bending stiffness $\bar{EI}_{\text{islands}}$ obtained from Eqs. 1 and 2 for $n = 5$. The additional elastic properties beyond those given above are $E_{\text{Si}} = 130\ \text{GPa}$ and $\nu_{\text{Si}} = 0.27$.

Mechanics models give the distribution of strains and displacements in the islands. As shown in Fig. S3B, the out-of-plane displacements in bridges impose bending moments M (and axial force F) to the island. The bending energy in the island is obtained in terms of its out-of-plane displacement u via the plate theory. The PDMS substrate is modeled as a semiinfinite solid subjected to the surface displacement u , and its strain energy is also obtained in terms of u . The displacement u is expanded to the Fourier series, with the coefficients to be determined by minimizing the total energy. The bending strains in each layer of the islands are obtained from the curvatures, which are the second-order derivatives of u . The maximum out-of-plane displacements are very small ($< 0.4\ \mu\text{m}$), as are the strains ε_{yy} and ε_{zz} ($\approx 0.01\%$) in the Si layer. The strain ε_{yy} in the Si element reaches the peak near the interconnections in the y -direction, whereas the peak of ε_{zz} occurs near those in the z -direction.

Off-Axis Stretching. Off-axis stretching has two effects, namely the axis stretch along the bridge direction and the shear normal to the bridge direction. Such deformation is accommodated by lateral buckling, which is characterized by the sinusoidal function (for axial stretch) shown in Fig. S34, and Bessel function (for shear). The out-of-plane rotation ϕ due to lateral buckling takes the form

$$\phi = B \left[\sqrt{\frac{2}{L_{\text{bridge}}}} z J_{-1/4} \left(\frac{13.96403}{L_{\text{bridge}}^2} z^2 \right) - J_{-1/4}(3.49101) \right] \quad [4]$$

for the symmetric buckling mode, and

$$\phi = B \left[\sqrt{\frac{2}{L_{\text{bridge}}}} z J_{1/4} \left(\frac{18.45820}{L_{\text{bridge}}^2} z^2 \right) + \frac{424.956}{L_{\text{bridge}}^3} z^3 \phi_p \left(\frac{18.45820}{L_{\text{bridge}}^2} z^2 \right) \right] \quad [5]$$

for the asymmetric mode, where $J_\alpha(x)$ is the Bessel function of order α , B is the amplitude to be determined by energy minimization, and $\phi_p(x)$ takes the form

$$\phi_p(x) = -\frac{1}{48x^2} \left[\begin{array}{l} 8^4 \sqrt{2^3} x^{9/4} \text{Hypergeom} \left(\frac{3}{4}, \frac{5}{4}, \frac{7}{4}; -\frac{1}{4} x^2 \right) \\ J_{-1/4}(x) \Gamma \left(\frac{3}{4} \right) - 6 \sqrt{2} \pi x^2 J_{1/4}(x) J_{-1/4}(x) \\ + 6 \sqrt{2} \pi x^{7/4} J_{1/4}(x) J_{3/4}(x) \text{LommelS1} \left(\frac{1}{4}, \frac{7}{4}, x \right) \\ - 9 \sqrt{2} \pi x^{3/4} J_{1/4}(x) J_{3/4}(x) \text{LommelS1} \left(\frac{5}{4}, \frac{3}{4}, x \right) \\ + 6 \sqrt{2} \pi x^{7/4} J_{1/4}(x) J_{-1/4}(x) \text{LommelS1} \left(\frac{5}{4}, \frac{3}{4}, x \right) \end{array} \right], \quad [6]$$

where $\text{Hypergeom}(a_1, a_2, \dots; b_1, b_2, \dots; x)$ is the generalized Hypergeometric function, $\Gamma(x)$ is the Gamma function, and $\text{LommelS1}(\mu, \nu, x)$ is the Lommel function. Here, $a_1, a_2, \dots, b_1, b_2, \dots, \mu, \nu$ are the parameters for the special functions.

We first obtain the solution for the bridges subjected to the off-axis stretching by energy minimization (including twisting energy) with respect to two amplitudes A and B . The reaction forces, bending moment, and torques at the bridge/island interconnections are then applied to the islands to determine the distributions of strains and displacements in islands.

Principal Strains. For the structure subjected to ε_{yy} , ε_{zz} , and ε_{yz} , the principal strains are

$$\varepsilon_{1,2} = \frac{\varepsilon_{yy} + \varepsilon_{zz}}{2} \pm \sqrt{\left(\frac{\varepsilon_{yy} - \varepsilon_{zz}}{2} \right)^2 + 4\varepsilon_{yz}^2}. \quad [7]$$

The principal strain presented in the article is ε_1 .

Twisting. Twisting shown in Fig. 3 is different from the off-axis stretching because it doesn't involve lateral buckling. For the multilayer stacks shown in Fig. S1 (stack width \gg stack thickness) subjected to a torque M_x , only the shear strain ε_{yz} exists and is given by (2)

$$\varepsilon_{yz} = \frac{M_x}{\overline{GJ}} x, \quad [8]$$

where \overline{GJ} is the equivalent torsional stiffness and given by

$$\overline{GJ} = 4w_s \left[\sum_{i=1}^n G_i h_i \left(b - \sum_{j=1}^i h_j \right)^2 + \sum_{i=1}^n G_i h_i^2 \left(b - \sum_{j=1}^i h_j \right) + \frac{1}{3} \sum_{i=1}^n G_i h_i^3 \right], \quad [9]$$

where G_i is the shear modulus for each layer.

Spacing Effect on Stretchability of Pop-Up Interconnect Structure. Fig. S5 shows the interconnect structure with the bridge of length L_{bridge}^0 and island of length L_{island}^0 . The bridges pop up after the prestrain releases and the bridge length L_{bridge}^0 changes to L_{bridge} , but the island length remains essentially unchanged because the elastic rigidity of island is many times larger than that of bridges. The prestrain at the system level of the pop up structure is then

$$\text{given by } \varepsilon_{pre} = \frac{L_{\text{bridge}}^0 - L_{\text{bridge}}}{L_{\text{island}}^0 + L_{\text{bridge}}^0}.$$

Let $\varepsilon_{\text{fracture}}$ ($\approx 1\%$) denotes the critical strain of fracture of bridge material, the maximum prestrain that can be applied in the system is given by

$$(\varepsilon_{pre})_{\text{max}} = \frac{L_{\text{bridge}}^0}{L_{\text{island}}^0 + L_{\text{bridge}}^0} \left(\frac{L_{\text{bridge}}^0 \varepsilon_{\text{fracture}}}{2\pi h_{\text{bridge}}} \right)^2, \quad [10]$$

where h_{bridge} is the bridge thickness, and it clearly shows that large spacing (i.e., L_{bridge}^0) and small bridge thickness increases the maximum prestrain at the system level. The stretchability of system is simply $(\varepsilon_{pre})_{\text{max}} + \varepsilon_{\text{fracture}}$.

1. Gray D, Hoa SV, Tsai SW (2003) *Composite Materials: Design and Applications* (CRC Press, Boca Raton, FL).

2. Timoshenko SP, Goodier JN (1987) *Theory of Elasticity* (McGraw-Hill, New York), 3rd Ed.

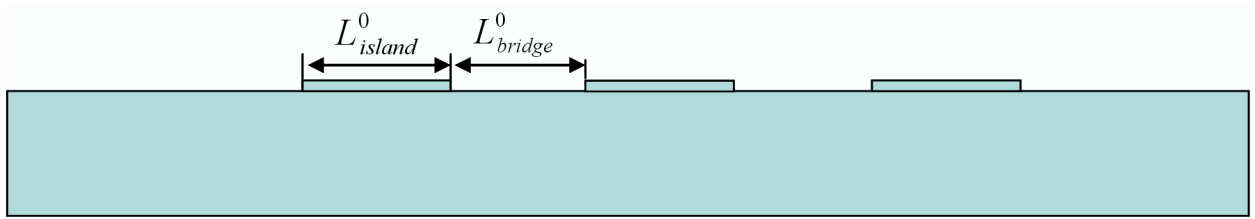
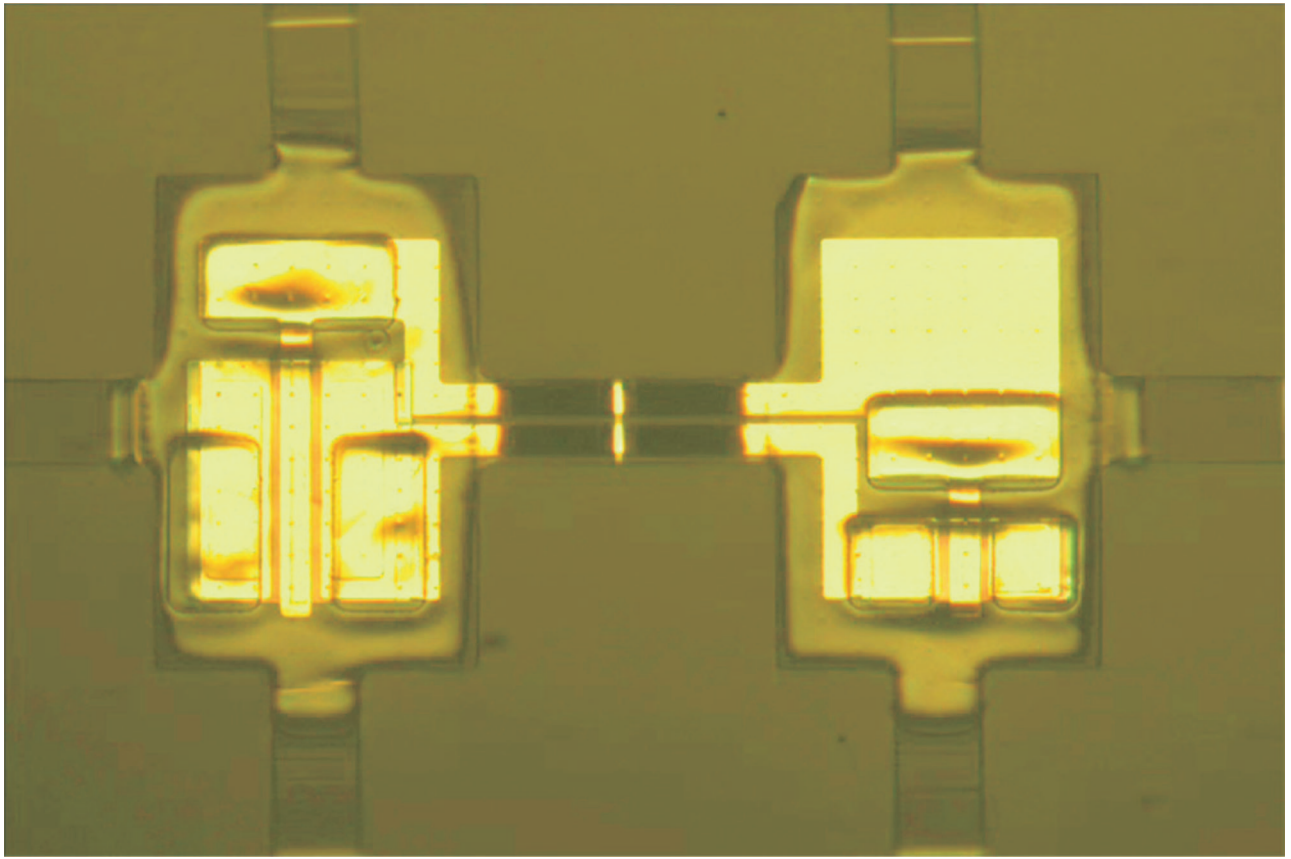
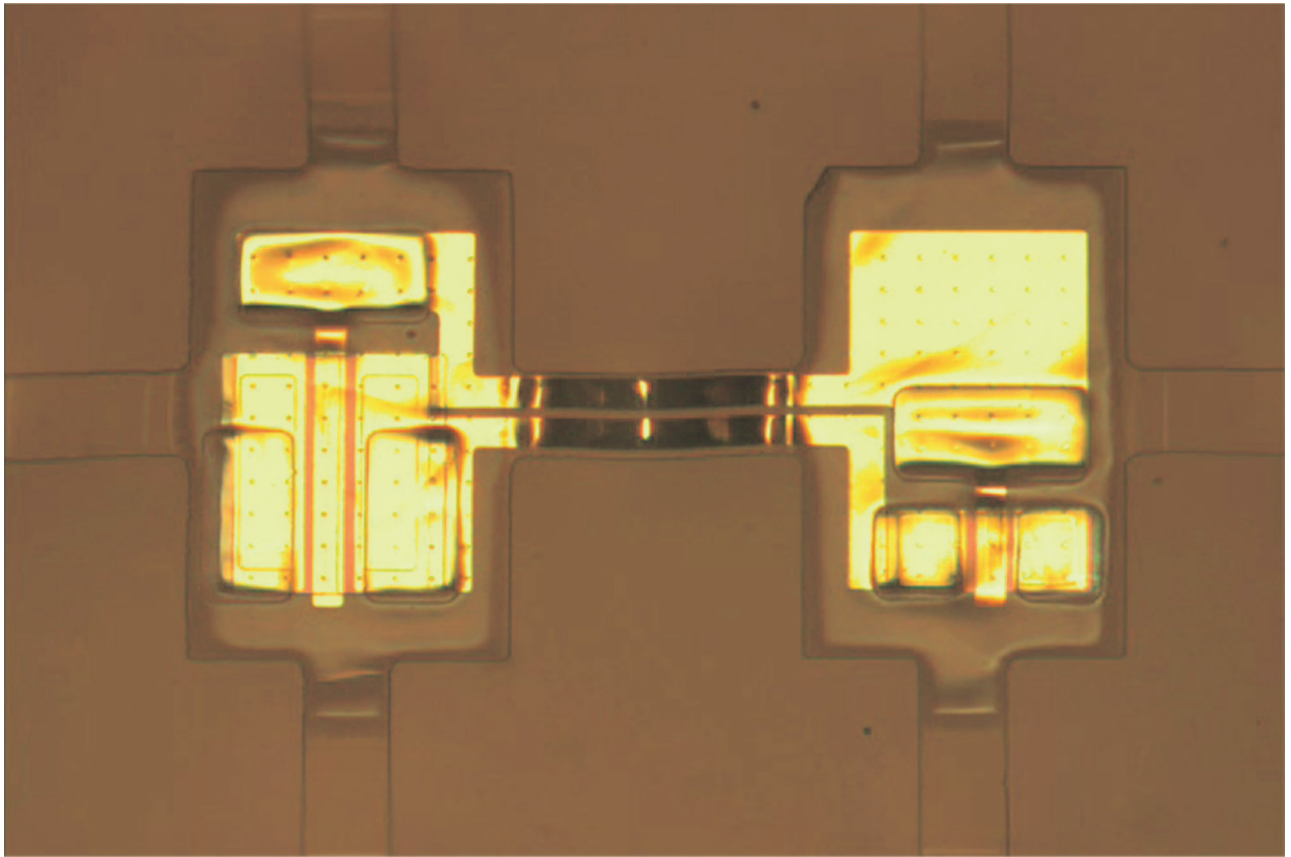


Fig. S5. Schematic diagram of island-bridge structure



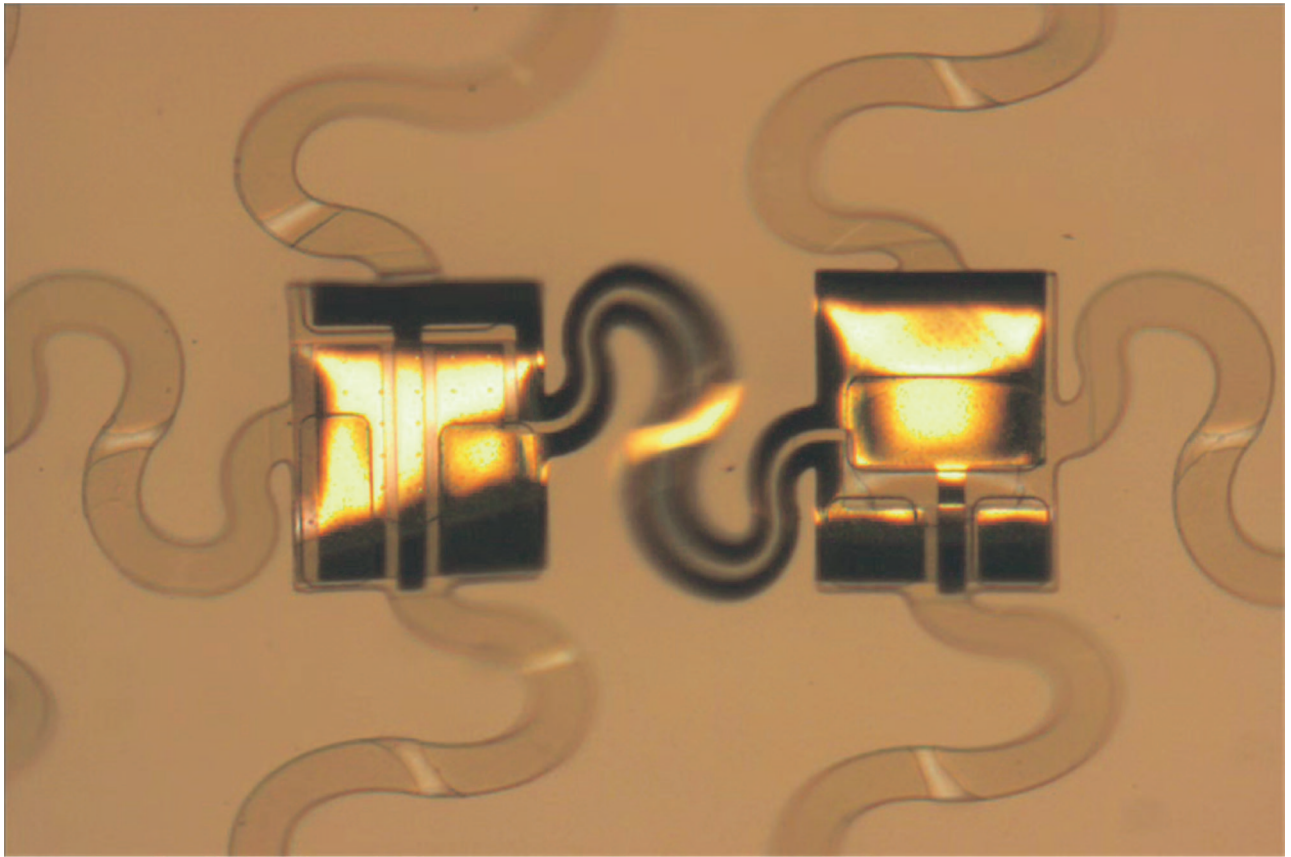
Movie S1. Stretching of pop-up inverters before PDMS encapsulation.

[Movie S1 \(WMV\)](#)



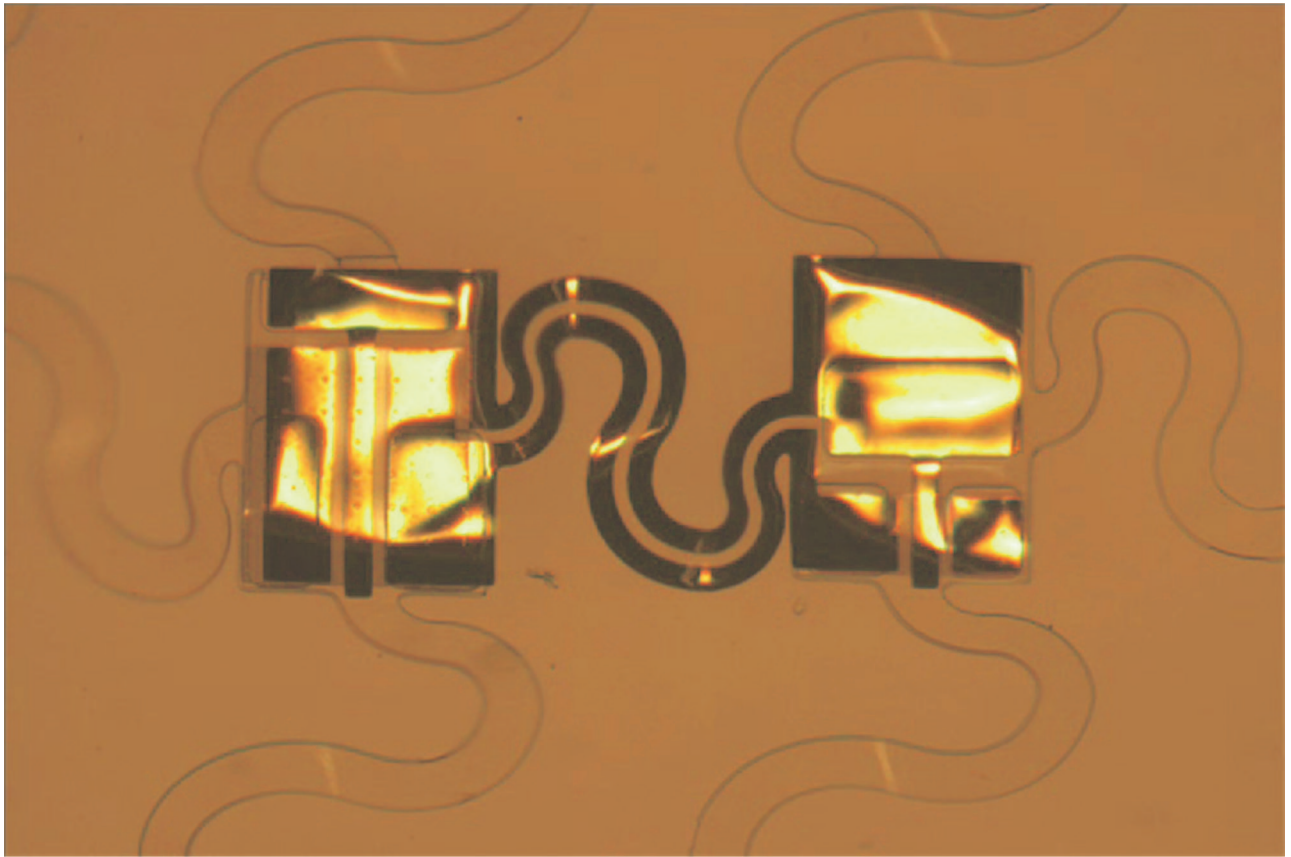
Movie S2. Stretching of pop-up inverters after PDMS encapsulation.

[Movie S2 \(WMV\)](#)



Movie S3. Stretching of pop-up inverters with S-shape bridges before PDMS encapsulation.

[Movie S3 \(WMV\)](#)



Movie S4. Stretching of pop-up inverters with S-shape bridges after PDMS encapsulation.

[Movie S4 \(WMV\)](#)